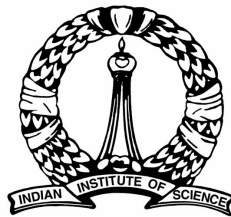


# *Integrable Vein Viewing System in Hand Held Devices*



**Phaneendra K. Yalavarthy**

[Supercomputer Education and Research Centre \(SERC\)](#)

*Indian Institute Of Science, Bangalore*

**Koushik Kumar Nundy**

Dept. of Electronics and Communication Engineering

*National Institute Of Technology.*

*Durgapur.*

**Shourjya Sanyal**

Dept. of Biotechnology.

*National Institute Of Technology.*

*Durgapur.*

## **ACKNOWLEDGEMENT**

*We would like to express our gratitude to Prof. Dr.S.Asokan (Professor, Department of Instrumentation, IISc Bangalore), and his students for extending lab facilities and providing technical support. We would especially like to thank Dr. Rajam Sekar (Project Associate, Department of Instrumentation, IISc Bangalore) for her constant help and guidance. We would also like to extend our thanks to the authorities of Supercomputer Education and Research Center, IISc Bangalore for allowing us to use their laboratory and computing facility.*

*The report would not have been possible without the moral and technical support from Dr. Amit Kumar Ghosh, for accomplishing phase I clinical trials and we take this opportunity to thank him heartily. We are also thankful to Mr.Tuhin Chatterjee. Lastly we will always be grateful to family and friends for their constant encouragement and support.*

***Phaneendra K. Yalavarthy***

***Koushik Kumar Nundy***

***Shourjya Sanyal***

# ***CONTENTS***

<b>Topic.</b>	<b>Page.</b>
<i>Acknowledgment.</i>	
<i>Table of contents.</i>	
<i>List of tables.</i>	
<i>List of figures and illustrations.</i>	
<b>Chapter 1 – Abstract.</b>	<b>1</b>
<b>Chapter 2 -Introduction.</b>	<b>2</b>
<b>Chapter 3 -Method.</b>	<b>3</b>
a. Intensity decay patterns of single LEDs	
b. Intensity decay patterns for multiple LEDs	
c. Camera Diameter	
<b>Chapter 4 - Results &amp; Discussion</b>	<b>7</b>
a. Single LED intensity decay behavior.	
b. Multiple LED intensity decay behavior.	
c. Optimal field of view for each camera set	
<i>I. Area of illumination using LED sets</i>	
<i>II. Field of view of Cameras used</i>	
d. Intensity against type of LEDs.	
e. Reasons for optimising at 780 nm.	
f. Reasons for optimising at 3 LED sets.	
g. Angles used for experimentation (hence, axial distance from focus)	
h. Optical Properties of Human skin and blood.	
<b>Chapter 5 – Optimized system</b>	<b>18</b>
a. System parameters	
b. Image quality and variance	
c. Possible improvements	
<b>Chapter 6 - Comparison with available technologies.</b>	<b>23</b>
<b>Chapter 7 - Conclusion and Future scope.</b>	<b>24</b>
<b>References.</b>	<b>25</b>
<i>Annexure I : Radiant power Energy Meter Details</i>	<b>28</b>
<i>Annexure II: Diode Details</i>	<b>31</b>

## **LIST OF TABLES**

### **CHAPTER 4.**

*Table 4.1 List of LED sets and circuit specifications*

*Table 4.2 Area of Illumination for LED set 4 (780nm $\times$ 4)*

*Table 4.3 List of camera specifications and field of view.*

*Table 4.4 List of focal distances.*

*Table 4.5 Quarter Millimolar Absorptivities, in  $l\text{ mmol}^{-1}\text{ cm}^{-1}$ , of the haemoglobin species from 620 to 940nm.*

*Table 4.6 Optical properties at  $\sim$ 780nm*

## **LIST OF FIGURES AND ILLUSTRATIONS**

### **CHAPTER 3.**

*Fig .3.1 - Setup for Single LED power decay measurement with axial distance.*

*Fig .3.2 - Setup for Multiple LED power decay measurement with axial distance.*

*Fig .3.3 - Displaying actual setup with multiple LED sets.*

*Fig .3.4 - Graph showing  $y = \cos x$ .*

*Fig .3.5 - The concentric LED array used with 1.5 cm radius.*

### **CHAPTER 4.**

*Fig 4.1. Single LED's power decay with increasing axial distance for 940nm, 840nm and 780 nm.*

*Fig 4.2. Actual and Normal power versus axial distance for set 1.*

*Fig 4.3 Actual and Normal power versus axial distance for set 2.*

*Fig 4.4 Actual and Normal power versus axial distance for set 3*

*Fig 4.5 Actual and Normal power versus axial distance for set 4*

*Fig 4.6 Area of Illumination for LED set 4 vs Dist from source*

*Fig 4.7 Intensity versus wavelength*

*Fig 4.8 Absorption coefficient of epidermis with  $f.mel = 10\%$*

*Fig 4.9 Absorption coefficient of whole blood (45% hematocrit).  
RED = oxy-hemoglobin, BLUE = deoxy-hemoglobin.*

*Fig 4.10 Reduced scattering coefficient,  $\mu_s'.derm$ , of dermis.*

*Fig 4.11 Scattering coefficient vs wavelength of oxygenated and deoxygenated whole blood computed by Mie theory using the calculated complex refractive indices.*

*Fig 4.12 Absorption coefficient vs wavelength of oxygenated and deoxygenated whole blood. Gray curves: data from Ref. [15]. Black curves: Mie calculations.*

## **CHAPTER 5**

*Fig 5.1 A three dimensional image of the optimized system.*

*Fig 5.2 Mobile with contraption (Back View).*

*Fig 5.3 Mobile(Front View) with contraption (Back View).*

*Fig 5.4 Mobile (Back View) with contraption (Front View)*

*Fig 5.5. Images obtained with device and 3MP camera without IR illumination, with illumination, with illumination after thresholding, for Fair complexion and Dark complexion skin.*

*Fig 5.6 Imaging technique.*

---

## Chapter 1 - Abstract

---

This is a feasibility study of a design where we use illumination in the Near Infrared range (NIR) and standard mobile phone camera systems to built a highly portable and cost efficient vein detection system. The system is tested using three camera-equipped cellphones of varying price and resolution ranges. We use cameras with VGA(640x480), 1.3MP (1280x1024) and 3MP (2048x1536) resolutions. The illumination is in form of multiple LED systems of certain wavelengths (780 nm, 840 nm and 940 nm ) in the NIR spectral region. We optimised a best case scenario with a system of 3 LEDs of 780nm for vein viewing. The work was accredited by an independent medical board based on field data.

---

## Chapter 2 – Introduction

---

There are several devices that find usage in the biomedical and biometric application sector. They are used to monitor behavior or patterns of biological systems, for purposes including identification, diagnosis and mapping.

An upcoming field which shows promise is that of vein detection techniques. There have been several methods that have been proposed and explained in recent literature, including but not limited to Near Infrared Region(NIR) imaging[1][2][3][8], multispectral imaging[4], Radio Frequency[6], NMR and ultrasound[7] among others. Each comes with its own sets of advantages and limitations.

However most such systems are extremely bulky or prohibitively costly, sometimes both. Also, they often require dedicated stand alone systems, which require specialized training and setup at a specific location, suitable for use only in hospital like environments and pathological laboratories, with obvious lack in mobility and of flexibility in use.

Also, several such setups are suitable for a limited purpose, resulting in a non-holistic approach, as in [2], [5] & [10]. Furthermore, advanced image processing techniques and/or signal analysis requirements go hard on their processing requirements, resulting in requirement of PCs, oscilloscopes, etc to complete the setup[1][3][4][9].

There are also certain limitations specific to the equipment and setups used. For e.g., in [1] there is a distinct possibility of "light spots", leak of energy due to the high scattering and a possibility of direct illumination from the LEDs.

In [3] and [4], multiple screens, images and cameras are required. This results in further escalation of cost, and rise in data acquisition time.

Here, we propose an extremely low cost, novel solution to the issue of vein imaging, using a device that is integrable with and utilizes mobile phone cameras for surface vein detection and imaging. It utilizes the property of differential absorption of Near Infrared light by oxygenated and deoxygenated blood over normal tissue.

We shall use illumination from NIR LED sources to illuminate the body surface, and take photographs of the illuminated area using a mobile camera device.

---

## Chapter 3 - Method

---

### a. Intensity decay patterns of single LEDs

There were three different LEDs used producing peak wavelengths of 780nm, 840 nm and 940 nm were used. The aim of the experiment is to find the power decays of the LEDs with the increasing axial distance from the source.

The power meter was used to compute the amount of incident IR from the LED. The power meter was clamped to a fixed plank perpendicular to the plank. The whole setup was colored black to decrease reflection from stray rays.

Three sets of readings were taken of power versus axial distance, for the three types of LEDs used.(For LED details refer Annexure II). The single LEDs were attached on a vero board and made at same axial height as that of the power meter incident window. The LEDs were connected via a crocodile clip to the current source, and voltage was adjusted to give optimum illumination of the LEDs.

The power meter was set up for reading, the power for the particular peak range of the LEDs used. A Radiant Power Energy Meter, with Model 70260 photodiode heads, from Spectra-Physics, were used to take power measurements of the single LEDs (For details regarding handling and operation of Energy meter and the photodiode head look into Annexure I). The power meter was re-set every time to reduce instrumental aberration. The LEDs apparatus was moves 0.5cm from 2 to 10 cm range. This was used to give us a practical idea about the power decay of the specific LEDs, within practical limits.

The experiment was repeated three times for each LED sets and the average result was computed,

The ideal result was computed and the variance was computed, to give an idea about the practical stochastic limits of the observed data.

The theoretical value was computed using the formulae

$$y \propto e^{-\mu x}$$

Where y = normalized power

x = distance from source

$\mu$  = absorption coefficient

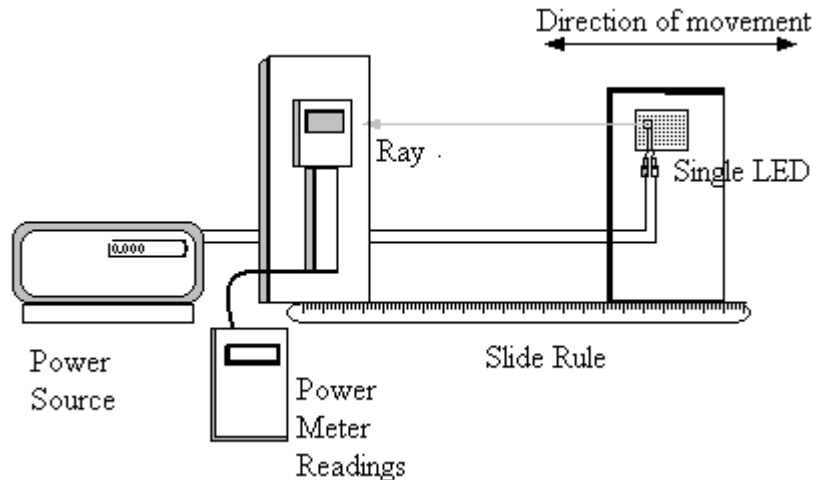


**Fig.3.1.** Setup for Single LED power decay measurement with axial distance.

### b. Intensity decay patterns for multiple LEDs

The procedure is similar to the single LED sets only that an array of 3-4 LEDs were used in series to do the experiment in place of single LED. The LEDs were mounted such that their focus lie on the axis of the power meter.

. A Radiant Power Energy Meter, with Model 70260 photodiode heads, from Spectra-Physics, were used to take power measurements of the single LEDs (For details regarding handling and operation of Energy meter and the photodiode head look into Annexure I). The power meter was re-set every time to reduce instrumental aberration. The LEDs apparatus was moves 0.5cm from 2 to 10 cm range. This was used to give us a practical idea about the power decay of the specific LEDs, within practical limits. The power meter was used to compute the amount of incident IR from the LED. The power meter was clamped to a fixed plank perpendicular to the plank. The whole setup was colored black to decrease reflection from stray rays.

The LEDs power versus axial distance from source was computed in four sets, 3 LEDs of 940nm, 3 LEDs of 840 nm and 3 and 4 LED set of 780nm. (For LED description sees Annexure II.) The LED sets were connected to a current source, with optimized adjusted voltage for the each LED to give maximum illumination. Each set was placed on a flexible bidirectional movable setup that kept the focus of the LEDs on the axis of the power meter receiver element.

The contraptions with the LEDs were moved from 2cm to 10cm, keeping focus on the axial plane at a distance of 1cm and readings were recorded. Repeated readings were taken for each set and the best case results were tabulated.

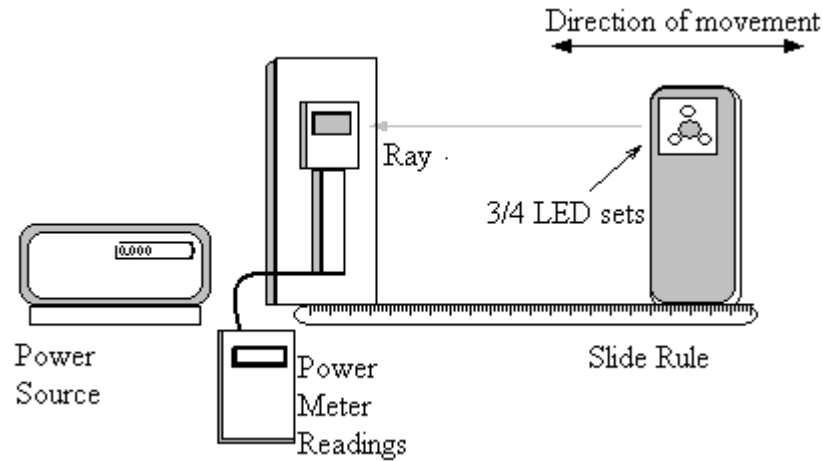


**Fig.3.2.** Setup for Multiple LED power decay measurement with axial distance.

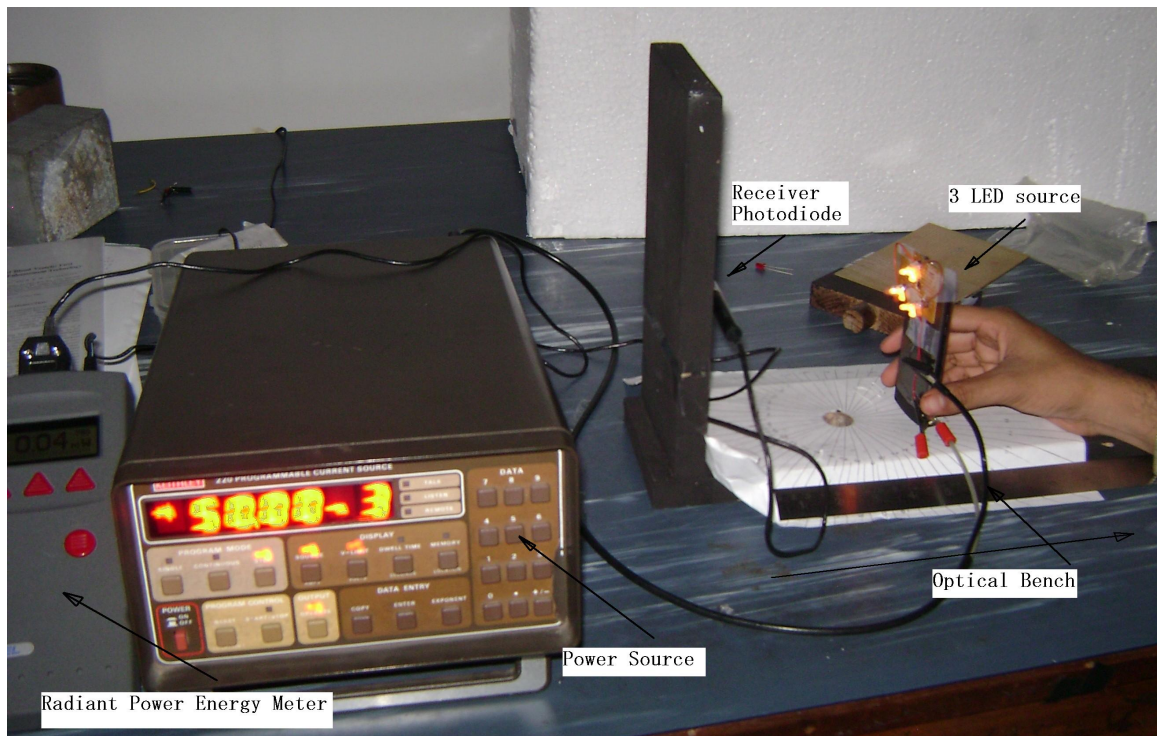


**Fig.3.3.** Displaying actual setup with multiple LED sets.

### c. LED array diameter.

*Crisan et al* have proved that concentric arrangement of LEDs though harder to implement, gives best overall diffusion and vein viewing capacities. So a concentric LED array was chosen over conventional parallel (double line, rectangular etc.) to optimize vein viewing of the instrument.

The diameter of the LED array was fixed at 1.5cm. This was based on the central idea that the closest feasible radius will help us to optimize the LEDs emitted power usage of the peak wavelength. The closest feasible radius is calculated by finding the maximum camera diameter of the available camera mobile devices.

The average camera apparatus radius varied in diameter from 1cm to 1.5 cm. This was based on market survey of available mobile camera phones of global and local brands like Sony Ericsson, Nokia, Samsung etc. The LEDs being 1cm in length the optimum bending angle was assumed to be between 1 to 0 cm so at optimum of 1.5cm radius was taken keeping practical feasibility conditions in nearest multiple of 0.5cm for convenience of construction.

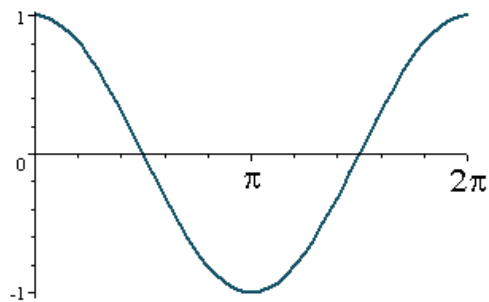


**Fig 3.4.**Graph showing  $y = \cos x$ .

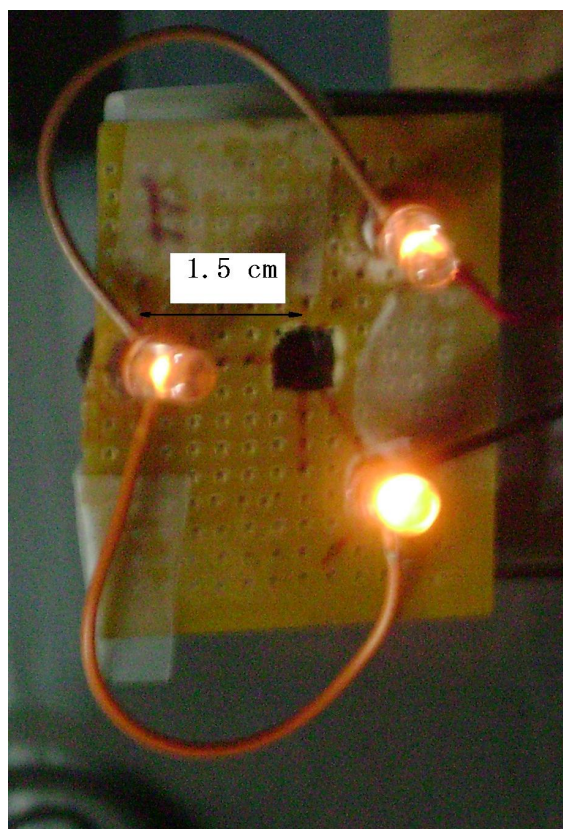


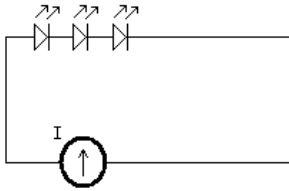
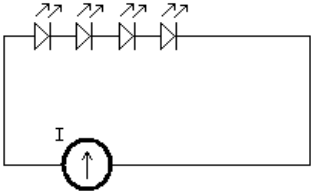
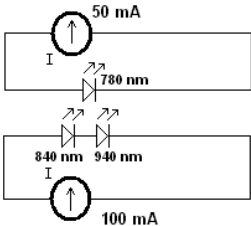
**Fig.3.5.** The concentric LED array used with 1.5 cm radius.

---

## Chapter 4 – Results and Discussions

---

In the following discussion the setups used are:

Set No.	LED wavelength	No of LEDs	Circuit Diagram	Rating
1	780	3		50mA, 6V
2	840	3		100 mA, 6V
3	940	3		100 mA, 4V
4	780	4		50mA, 8V
5	780+840+940 0	1+1+1		See ckt.

**Table 4.1** List of LED sets and circuit specifications

### a. Single LED intensity decay behavior

We can see that for a single LED, the observed decay pattern is, as suggested in theory, nearly exponential in nature. The tendencies for the 780, 840 and 940nm single LEDs are as follows:

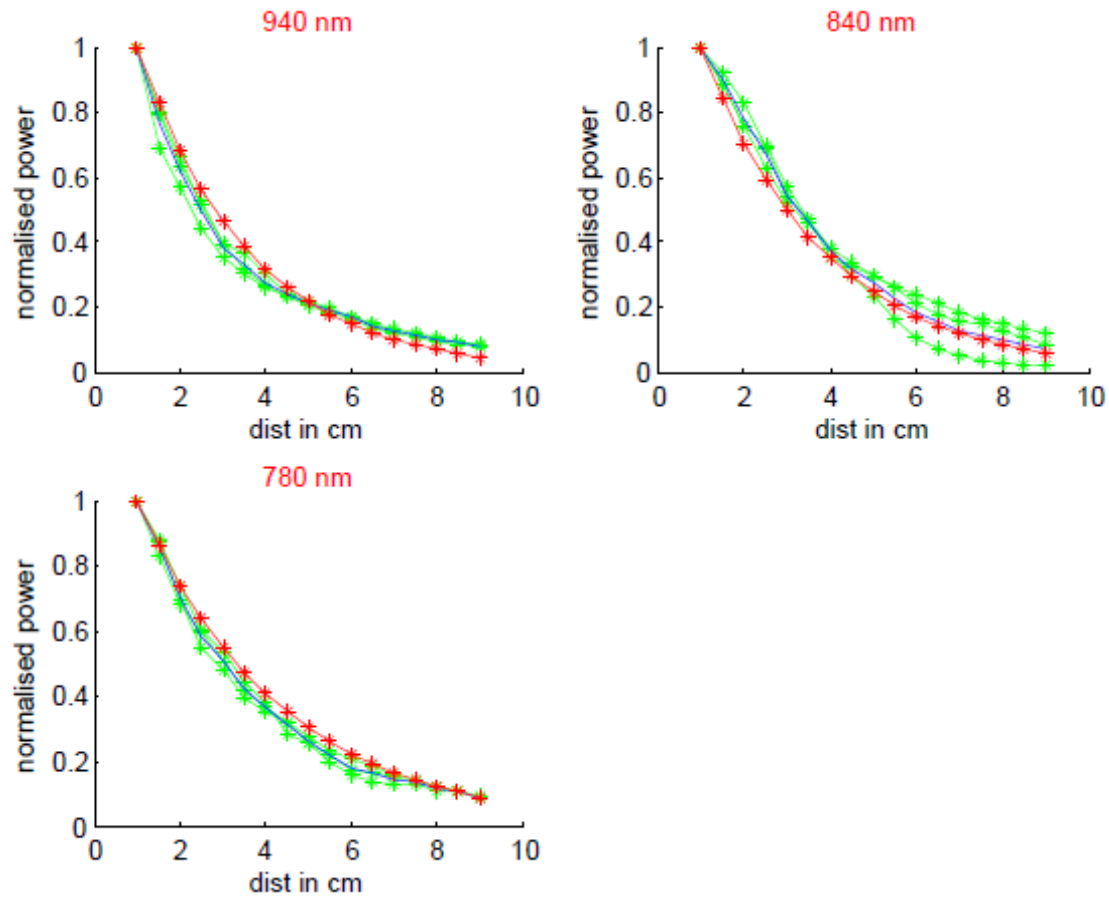


**Fig 4.1** Single LED's power decay with increasing axial distance for 940nm, 840nm and 780 nm.

The green lines represent the actual normalised power obtained on slowly moving the power meter from the source. The red line denotes the theoretical value, and the blue, the median of the observed values.

From the above graphs, we can see that a very close fit is observed between the expected and obtained values.

The theoretical values follow the curve

$$p = e^{-\mu \cdot x},$$

$$y = p/p_{\max}$$

where  $p$  = Actual power

$p_{\max}$  = Maximum intensity

$y$  = normalised power

$x$  = distance of power meter from source  
 $\mu$  = absorption coefficient  
 and the observed value for  $\mu \sim 0.42$ .

### b. Multiple LED intensity decay behavior

For sets of multiple LEDs, we see that the power obtained on the axis obtains a peak value at a certain distance, dropping off on either side in a more or less even, but non-linear manner. The graphs of normalised power against axial distance have been obtained from the following setup mentioned in the Method section.

The nature of the curves obtained is as follows:

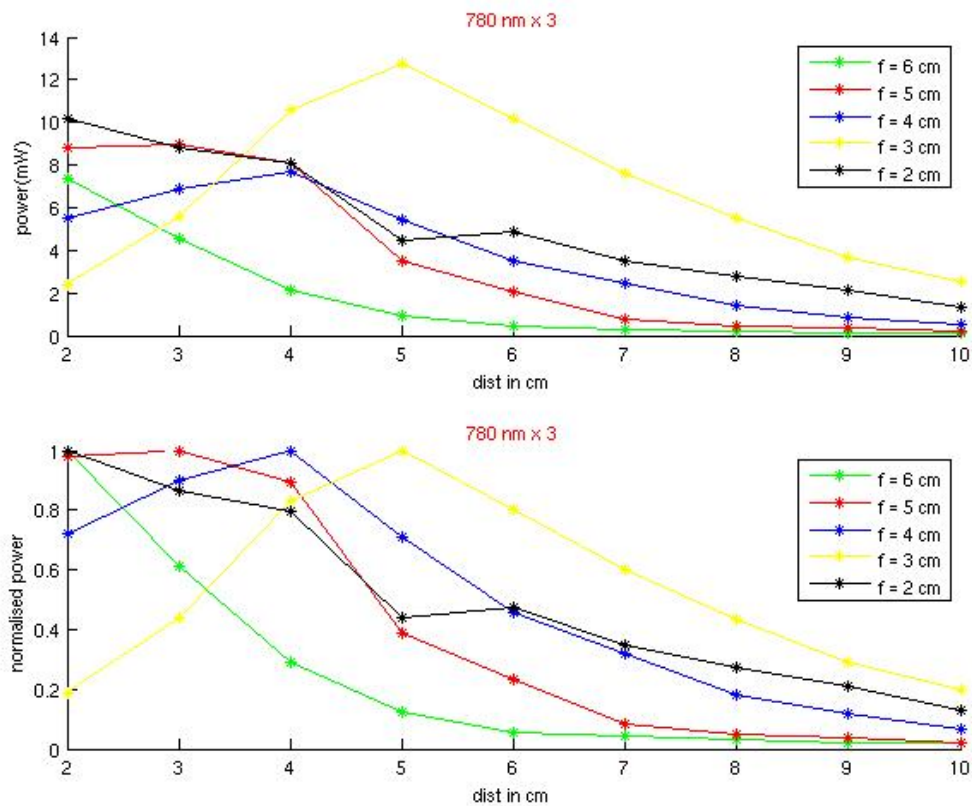


**Fig 4.2** Actual and Normal power versus axial distance for set 1.

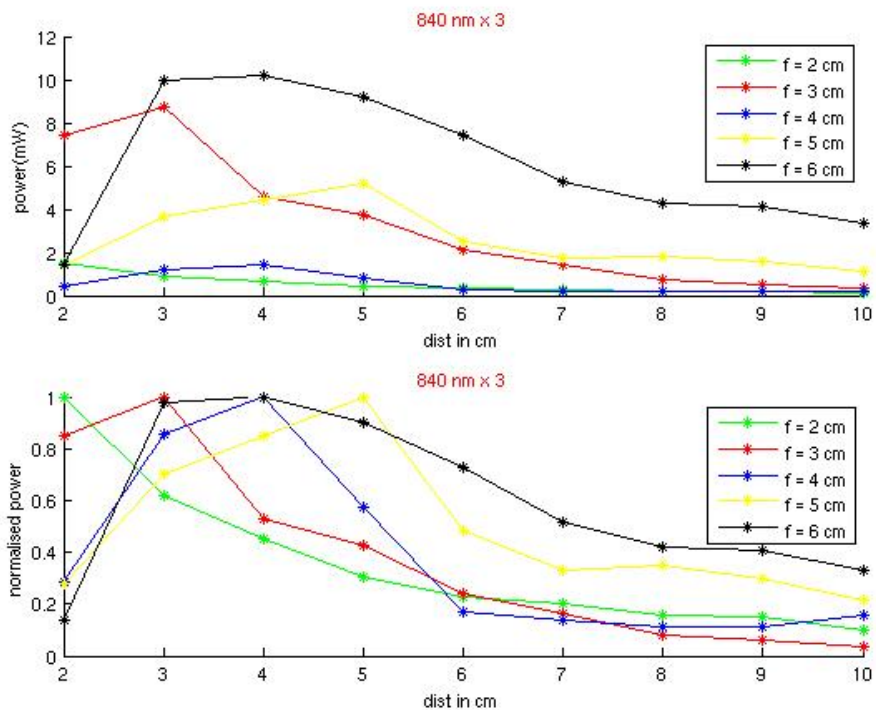


**Fig 4.3** Actual and Normal power versus axial distance for set 2.

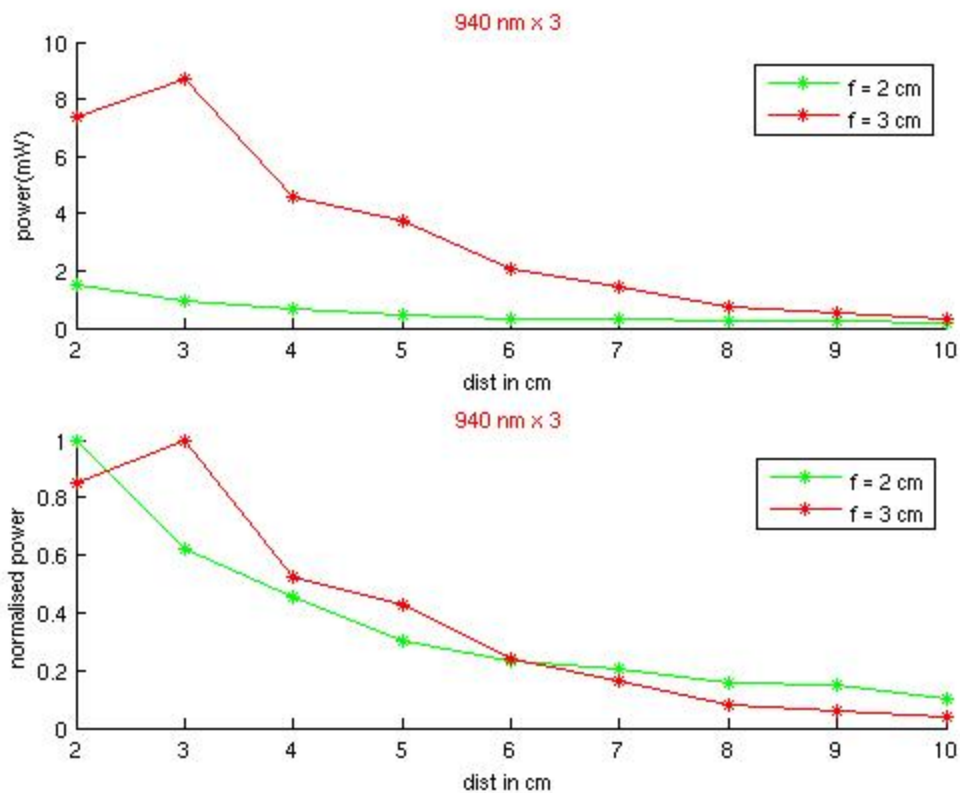


**Fig 4.4** Actual and Normal power vs axial distance for set 3.

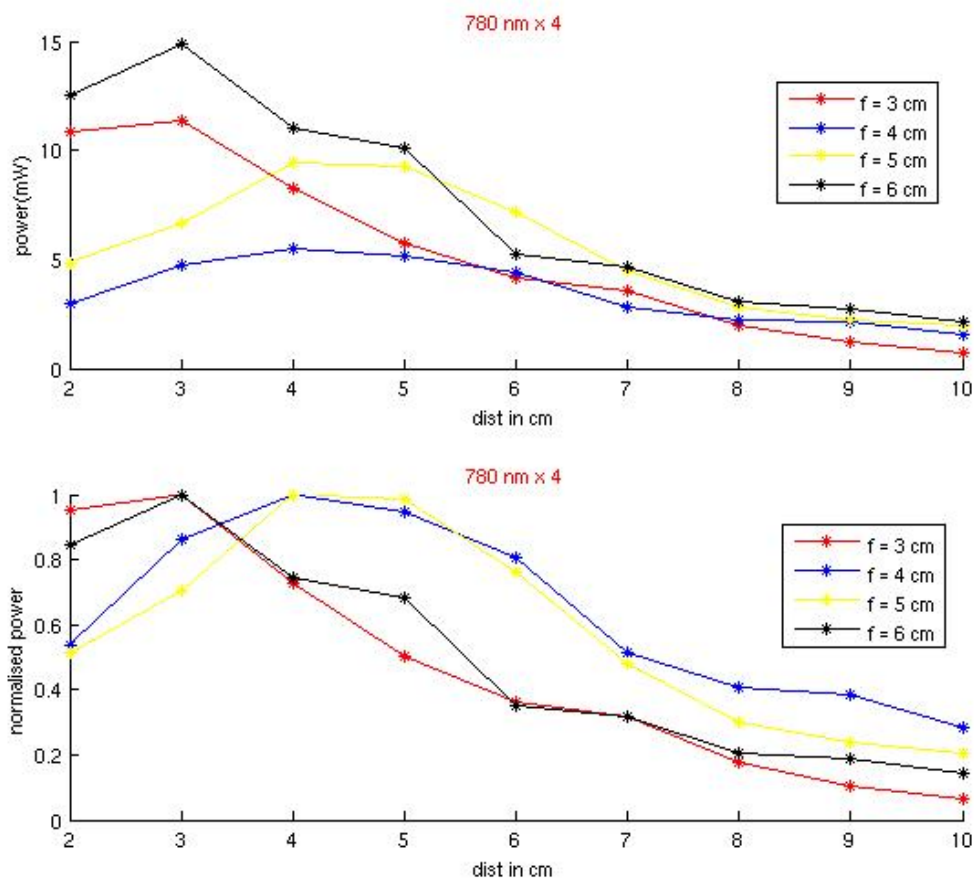


**Fig 4.5** Actual and Normal power versus axial distance for set 4

\*\* Axial focus : data1- 2cm , data2- 3cm , data3- 4cm , data4- 5cm , data5- 6cm.

Thus we can see that maximum power intensity is observed at focal distance for low distances. For higher distances, however, maximum intensity occurs at close regions, with a local maxima at focal distance, which is lower because of the power meter being quite far from the LED array source.

*(correlation of graph with image)*

We can expect clearer images to be obtained, if higher intensity illumination is provided, depending on the camera's properties, which limit the maximum intensity over which overexposure would occur resulting in noisy images. Also, below a certain minimum exposure, there is no detection of reflected radiation due to typically low

sensitivity of mobile phone cameras. There is the issue of a minimum distance below which the camera autofocus cannot function. Thus, the actual range of distances which provide acceptable images for use becomes limited.

**c. Optimal field of view for each camera set (Optimal area of illumination)**

**(I) Area of illumination using LED sets**

The area of illumination varies almost linearly with the distance of the LED array source from the illuminated region. Taking threshold at 0.05 of max possible intensity, we get area as below:

Distance from LED Tip	Total Number of Pixels	Threshold Limit	White Pixels	Black Pixels	Pixels in 1 cm <sup>2</sup>	Total area of Illumination
2	3145728	0.05	875257	2270471	148225	5.9
3	3145728	0.05	584752	2560976	99225	5.89
4	3145728	0.05	386016	2759712	62500	6.18
5	3145728	0.05	346116	2799612	55225	6.27
6	3145728	0.05	271352	2874376	40000	6.78
7	3145728	0.05	261980	2883748	36100	7.26
8	3145728	0.05	229294	2916434	30625	7.49
9	3145728	0.05	170434	2975294	22500	7.57
10	3145728	0.05	113420	3032308	14400	7.88

**Table 4.2** Area of Illumination for LED set 4 (780nm $\times$ 4)

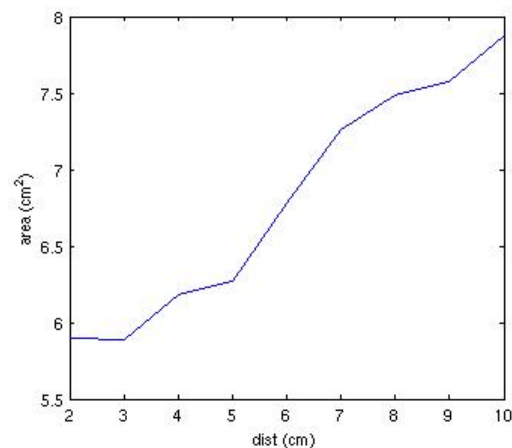


**Fig 4.6** Area of Illumination for LED set 4 vs Dist from source

### (II) Field of view of Cameras used

Manufacturer	Model	Resolution	Region(from 5 cm)	Area
Samsung	U700	3MP	5 cm x 4 cm	20 cm <sup>2</sup>
Nokia	6030	3.2MP	6.5 cm x 4.9 cm	31.8 cm <sup>2</sup>
Samsung	F679	1.3MP	4.6 cm x 3.2 cm	14.7 cm <sup>2</sup>
Motorola	L6i	0.3MP (VGA)	5 cm x 3.7 cm	18.5 cm <sup>2</sup>

**Table 4.3** List of camera specifications and field of view.

#### d. Intensity against type of LEDs

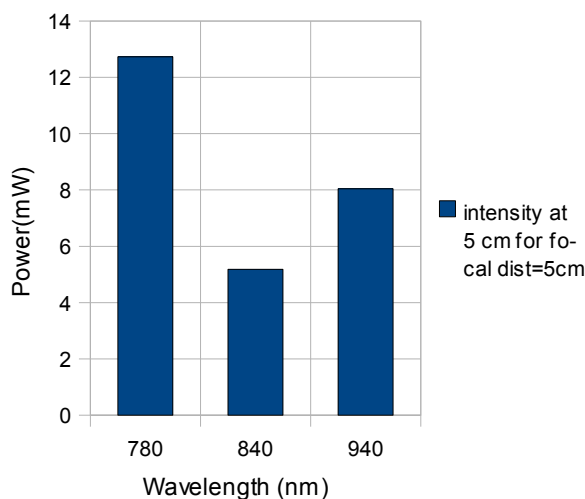


**Fig 4.7** Intensity versus wavelength.

We can see that there is considerably higher power in the 780nm x 3 LED set that we are using. This, typically, should lead to a rise in image quality courtesy higher intensity, constricted only by the aforementioned restrictions.

#### e. Reasons for optimising at 780 nm

We took images for sets 1, 2, 3, 4 and 5 with the 3MP camera. There were distinctly better images for sets 1, 4 and 5 when compared to sets 2 and 3. Also, there is no discernible difference in image quality between set 1, 4 and 5. The circuit complexity, however, is much higher for set 5, because of the different wavelength LEDs having different current ratings. Thus, we can say that sets 1 and 4 are the best performing and most efficient setup in terms of feasibility and image quality.

#### **f. Reasons for optimising at 4 LED sets**

For sets 1 and 4, there is comparable performance in terms of image quality at medium distance ranges. However at slightly higher range, illumination suddenly drops off for set 1. Also, set 4 has a more regular illumination pattern, closely resembling a squircle. So, we prefer using set 4, the 780 nm x 4 LED set

#### **g. Angles used for experimentation(hence, axial distance from focus)**

To make the beams meet at a certain point on the axis, the LEDs are tilted at certain angles in respect to the horizontal. These angles are based on the axial distance at which the separate beams' central axes meet. The focal distances and angles of inclination we used are as follows:

Focal Distance (cm)	Angle (degrees) in respect to horizontal
2	53
3	63.5
4	69.5
5	73.3
6	79

**Table 4.4** List of focal distances.

#### **h. Optical Properties of Human skin and blood.**

The quality of image obtained by any camera is dependent on the optical properties of human tissue. This is because any image obtained depends not just on the light emitted by the LED source, but on the amount of light that is reflected back into the field of view of the camera.

The optical properties that primarily need to be considered are the absorption and scattering coefficients of skin epidermis, melanosomes(containing melanin) and venular blood at the required light wavelength (780 nm). Also required is the typical quantity of melanosomes in the epidermis of light skinned and dark skinned people. The melanin concentration would help calculate the ratio of absorption coefficients of skin to venular blood at 780 nm. This in turn, would help predict contrast pattern for images obtained with ambient lighting at 780 nm, for “Vein”：“other tissues”.

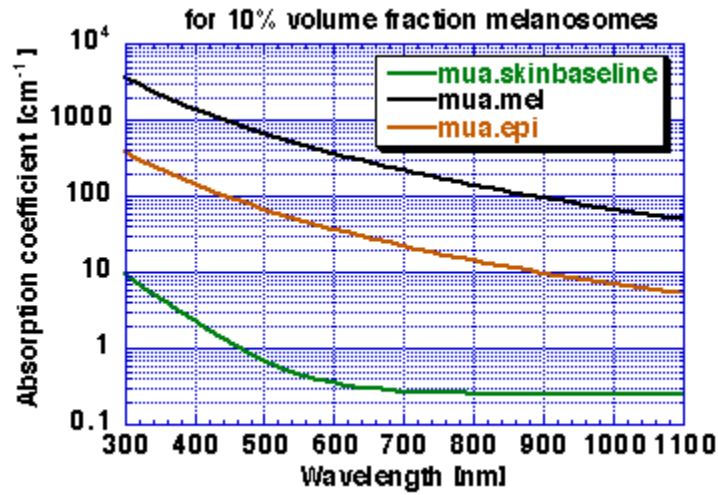


Fig 4.8 Absorption coefficient of epidermis with  $f_{\text{mel}} = 10\%$ [14]

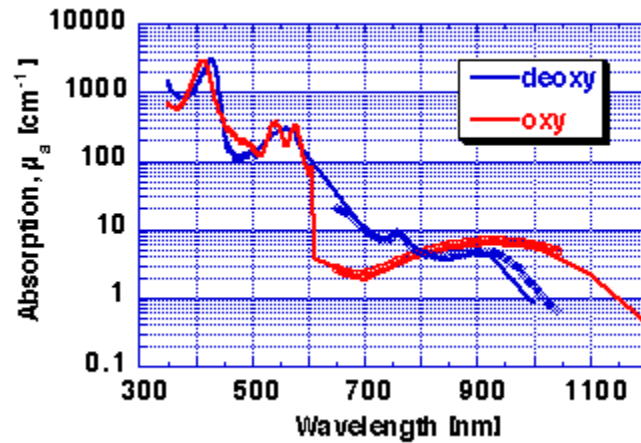


Fig 4.9. Absorption coefficient of whole blood (45% hematocrit).  
 RED = oxy-hemoglobin, BLUE = deoxy-hemoglobin.[14]

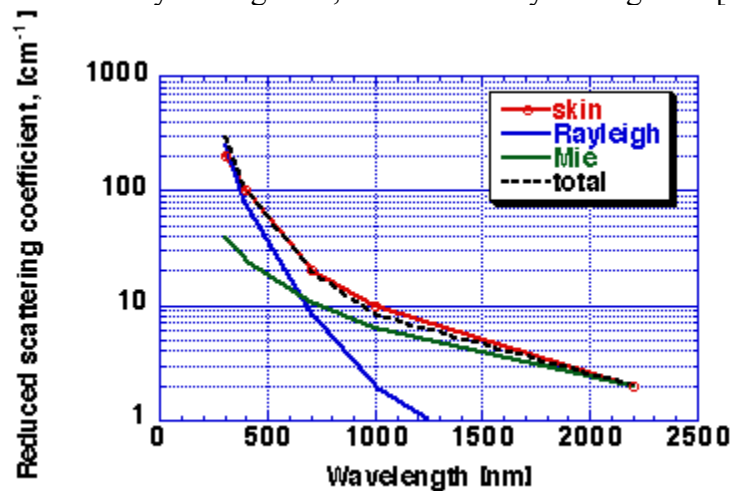
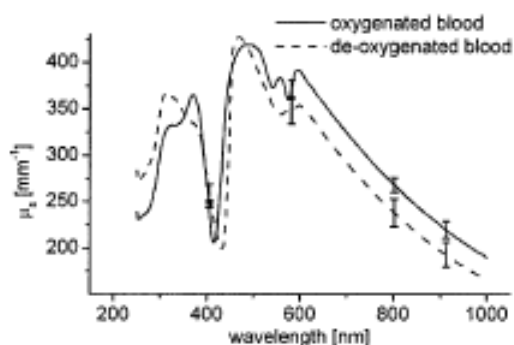
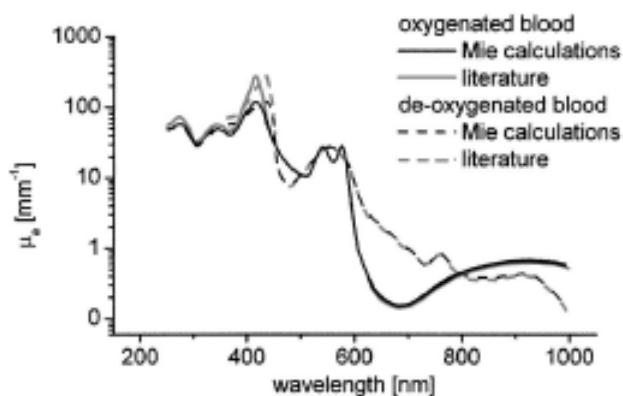


Fig 4.10 Reduced scattering coefficient,  $\mu_s'$ , derm, of dermis.[14]



**Fig.4.11** Scattering coefficient vs wavelength of oxygenated and deoxygenated whole blood computed by Mie theory using the calculated complex refractive indices.[12]



**Fig.4.12** Absorption coefficient vs wavelength of oxygenated and deoxygenated whole blood. Gray curves: data from Ref. [15]. Black curves: Mie calculations.[12]

**Table 4.5** Quarter M<sub>λ</sub> of the haemoglobin

$\lambda$ (nm)	O <sub>2</sub> Hb	Hb	COHb	metHb
620	0.27	1.46	0.39	3.14
630	0.19	1.22	0.27	3.21 (max)
650	0.12	0.98	0.14	1.56
660	0.10	0.90	0.10	0.79
690	0.09 (min)	0.61	0.05	0.16 (min)
720	0.11	0.43	0.04	0.16
736	0.12	0.40 (min)	0.04	0.18
760	0.15	0.45 (max)	0.04	0.23
800	0.20	0.26	0.03	0.37
815	0.22	0.24	0.03	0.42
850	0.26	0.22 (min)	0.03	0.54
880	0.29	0.23	0.03	0.61
910	0.30	0.24 (max)	0.03	0.69
930	0.30 (max)	0.22	0.03	0.73
940	0.30	0.21	0.03	0.74

Property	Skin	Vein (Deoxy-Hb)
Absorption coefficient $\mu_a$ ( $\text{mm}^{-1}$ ) [14]	0.05	0.9
Reduced Scattering coefficient $\mu_s'$ ( $\text{mm}^{-1}$ ) [12][13][14]	1.8	3.2
Anisotropic coefficient g [14][11]	0.78-9.94	0.99

**Table 4.6** Optical properties at ~780nm

Volume fraction of melanosome in skin:[14]

- light-skinned adults f.mel = 1.3-6.3%
- moderately pigmented adults f.mel = 11-16%
- darkly pigmented adults f.mel = 18-43%

The net epidermal absorption coefficient,  $\mu_{a,epi}$ , combines the baseline skin absorption and the melanin absorption and is calculated:

$$\mu_{a,epi} = (f.mel)(\mu_a.mel) + (1 - f.mel)(\mu_a.skinbaseline)$$

For example, a moderately pigmented adult with a 10% volume fraction of melanosomes will have absorption coefficients,  $\mu_{a,epi} = 0.0254$  at 755 nm.

So, we can see that expected contrast ratio should be around 17:1 for a medium pigmented adult for Vein : Skin.

---

## Chapter 5 – Optimized system

---

### a. System parameters

The camera mobile system is attached with an external contraption containing a concentric array of four LEDs in a circular symmetrical pattern, (i.e. each LED lies on the circumference of a circle and ninety degrees from the center). This setup was found to be the best case for vein viewing using minimal power consumption i.e. in our case an attached camera mobile device.

The set is made by arranging in a circle of a diameter of 3 cm inward bending LEDs with an angle of  $77^\circ$ .

The LEDs were fixed on a veroboard on LED holders. Each LED was 1 cm in height.

The contraption was connected to a 6V, (suggested current input 50 mA) external power source through a removable clip. The power source and the veroboard containing the LED array were fixed on a removable plastic cover. A 30% pass filter is added to cut glare and give optimum viewing capabilities.

The contraption is switched on/off by means of a removable clip.

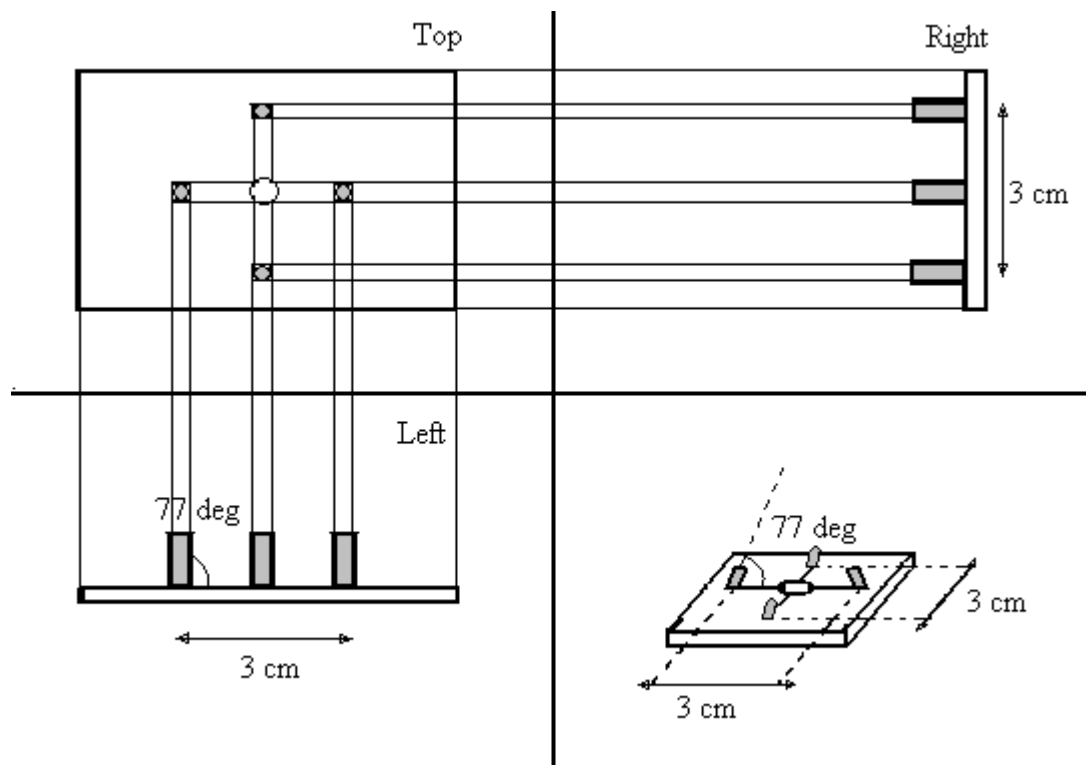


**Fig 5.1.** A three dimensional image of the optimized system.



**Fig 5.2.** Mobile with contraption (Back View).

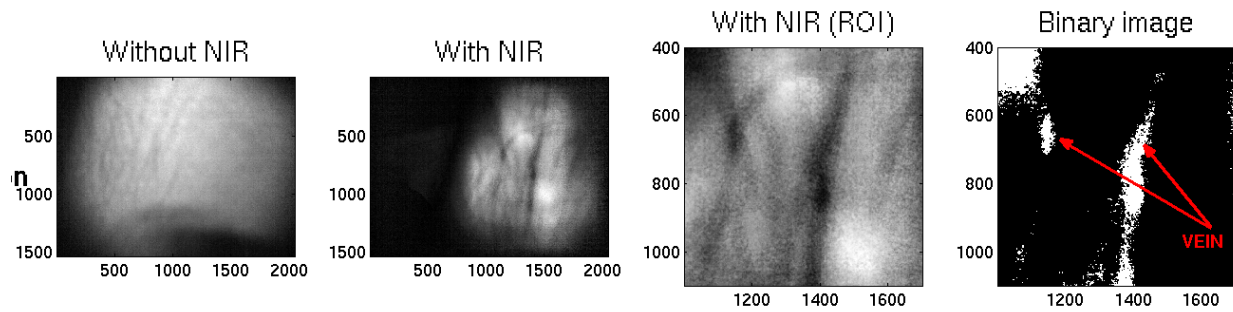


**Fig 5.3.** Mobile(Front View) with contraption (Back View).



Fig 5.4. Mobile (Back View) with contraption (Front View).

**b. Image quality and variance**  
**(a) Dark Complexion**



**(b) Light Complexion**

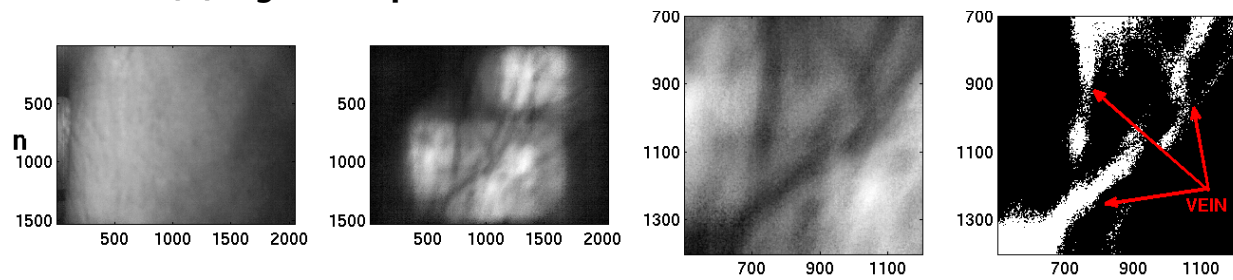


Fig 5.5. Images obtained with device and 3MP camera without IR illumination, with illumination, with illumination after thresholding, for Fair complexion and Dark complexion skin.

**Working Principle:** The near infrared light (784 nm) is sensitive to oxygenated hemoglobin in the blood, to provide the contrast between the blood vessels and skin. The penetrability of near infrared light is more compared to visible light making it ideal for vein detection. Four near infrared LEDs are used to provide uniform illumination and images will be acquired while these LEDs are on. The instrument was optimized and found to have good performance when the images were acquired at ~ 4 cm distance from the human skin.

**Safety Measures:** The equipment (Near infrared LEDs) is powered through four AA size batteries, providing 6 Volts (50 mA). The near infrared light is completely harmless and typical power reading of the near infrared light is 10 mW. All images are acquired non-invasively using mobile phone camera and there is no ionizing radiation involved.

**Image Acquisition time:** Patient preparation: ~ 1 minute, Acquisition: ~ 3 minutes (Three images will be acquired : one with LED illumination, second without LED illumination, third will be during intervensus injection)

**For further details regarding protocol refer to protocol details separately uploaded.**

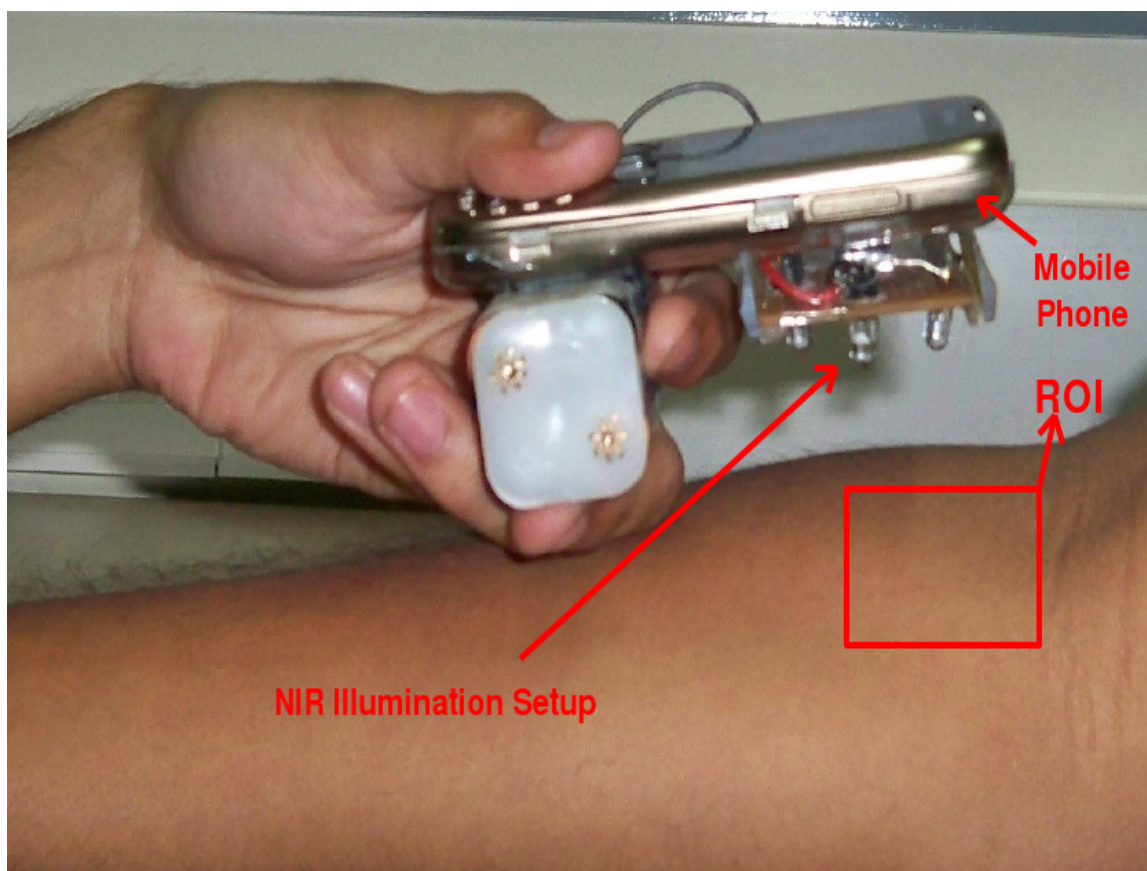


**Fig 5.6.** Imaging technique.

### **c. Possible improvements**

The current setup proves the hypothesis that current models of available mobile camera with suitable LED array can be optimized for dermal and near-dermal vein viewing. Possible optimization includes a thresholding algorithm, to give clearer indication of vein detection and indication. Also diffused light source can be used for more uniform illumination. Larger concentric LED arrays with similar focus as in the optimized system, will give better field of view for vein viewing.

The contraption could be integrated into the camera mobile phones to further enhance mobility and portability. The camera quality improvement will give better quality images. IR sensitivity of the camera could be further increased to give better quality images in the NIR domain.

It can be added to internal battery source could make the contraption less bulky.

---

## Chapter 6 - Comparison With Available Technologies

---

### a. Academic Publications

Refer to Chapter 2 - Introduction.

### b. Patented technologies

The patents mentioned in the references deal mostly with the issue of subsurface structure imaging methodologies and systems.

Patents 2, 3, 4, 5 and 6 which basically deals with the same invention under different jurisdictions, necessarily deal with generation of diffused infrared light for illuminating an object and producing a video image of the object based on reflected infrared light. While the described mechanism can be used for the purpose of vein imaging, its primary utility is in that of thermal imaging and also that of short range vision in dark ambience. Though similar in principle to the device/mechanism that has been discussed and presented in this report, it has several important points that helps us discern between the two.

A primary difference is in the mounting of LEDs on a curved pseudo spherical surface in the aforementioned patent literature. This results in increased complication of design and usage as space occupied also increases, especially when compared to the device in question, viz. Former is not well suited to be integrated in miniature hand held devices. It is hence observed that the proposed device has an higher portability and manoeuvrability. The number of LEDs used in constructing the device, in the above mentioned patents are much higher and therefore needs larger external power input to run device, which prevents it to be integrated to hand held devices containing minimal battery operated power source. More complex optical setup is required, using complex amalgamation of mirrors, lenses and multiple external light source to optimise performance, making it more bulky and not suitable as add-ons to hand held devices. Also, such a setup would result in escalation of cost and diminished ease of use.

For patents 7 and 8, we see a structure much complex in nature, with image processing algorithms introduced resulted in added requirement of processing power. Masking, division, contrast enhancement and blue filter cause an unwanted increase in bulk. Use of additional optical tools is an added problem.

For patent 9, dedicated digitizer image processor, and specific diagnostic and prognostic expert system circuitry is required, which results in massive increase in complexity and cost. Thus its usefulness is limited to pathological laboratories, hospitals and high cost setups. It lacks the capability to record information in pictographic format, thus rendering inability of data recovery and circulatory system mapping.

---

## Chapter 7 – Conclusion and Future Scope

---

Thus, we can see that we have arrived at a prototype model of a mobile camera integrable vein viewing device. At cost ranges of US\$ 10 or lower (excluding the mobile phone), it is an extremely low cost and versatile device. It requires no prior specialised training or expertise, and can various applications ranging from intravenous injection or blood drawing assistance, to mapping of surface veins.

The graphs generated for multiple LED sets give conclusive proof about 780nm peak wavelength having optimised sensitivity for the deoxygenated blood-containing vesicles near the cutaneous and dermal veins and venules, over other near infrared wavelengths in the 840 nm and 940nm peak wavelengths. The generated graphs give us an idea of optimal axial focus and distances. It is observed that for the LED angles to the horizontal greater than  $79^\circ$ , produced images are too diffuse in nature. So, they provide most uniform region of illumination.

The device has several notable advantages over present alternatives. There are a lot of distinct advantages on the described system, mostly in terms of mobility and ease of use. Also, cost effectiveness and simplicity of production can lead to a wide usage. The system, coupled with basic thresholding algorithms, promises to give medically acceptable quality images in small handheld devices containing at least 3MP image resolution and above.

There are also some limitations, however, to the device. The primary issue is that while the veins detected can be distinctly understood from the raw image, the image seems blurry and its detection of veins is not exhaustive, but suggestive. Also, there is little or no image processing involved resulting in difficulty of use for even the slightly visually impaired. Image may flicker depending on camera configuration, and is dependent on hand movement and stability. Image quality depends on external variables like ambient illumination and skin tone. The device is necessarily not an innately trustable medical aiding device at its current form. However, it is suitably functional for a prototype, with finer tuning possible. Some improvements have been suggested to the design in the 'Possible Improvements' section.

The device is a tested concept that current models of available mobile camera with suitable LED array can be optimized for dermal and near-dermal vein viewing. It successfully establishes the claim. Though further improvements may lead to successful commercialisation and development of the said product.

## **REFERENCES.**

- (1) Septimiu Crisan, Ioan Gavril Tarnovan, and Titus Eduard Crisan, "A Low Cost Vein Detection System Using Near Infrared Radiation", SAS 2007 - IEEE Sensors Applications Symposium, San Diego, California USA, 6-8 February 2007.
- (2) Frederick D. Scott Jr., Kyung A. Kang and G. M. Williams, "Diagnosis of Deep Vein Thrombosis with NIR Spectroscopy", Proceedings of The First Joint BME/EMBS Conference Serving Humanity, Advancing Technology, Oct. 13-16, Atlanta, GA, USA p-1101.
- (3) Yu Chengbo, Qing Huafeng and Zhang Lian, "A Research on Extracting Low Quality Human Finger Vein Pattern Characteristics", Proceedings of the 7th World Congress on Intelligent Control and Automation June 25 - 27, 2008, Chongqing, China.
- (4) F. P. Wieringa, F. Mastik, F. J. Ten Cate, H. A. M. Neumann and A. F. W. Van Der Steen, "Remote Non-invasive Stereoscopic Imaging of Blood Vessels: First In-vivo Results of a New Multispectral Contrast Enhancement Technology", Annals of Biomedical Engineering, Vol. 34, No. 12, December 2006, pp. 1870–1878.
- (5) M. Poon and C. Learra, "Imaging of the Pulmonary Veins in Patients with Atrial Fibrillation", Springer Book Chapter.
- (6) Peter J. Yim, Hani B. Marcos, Peter L. Choyk, Julia L. Hvizda, Steven K Libutti, Bradford J. Wood, "Detection of Blood Vessels for Radio-Frequency Ablation Treatment Planning", US. Government Work Not Protected by U S Copynght.
- (7) JM. Correas, O. Hilinon, M. Cherkaoui and JF. Moreau, "Ultrasound contrast agents: clinical applications", 1998 IEEE Ultrasonics Symposium, pp 1773-1778.
- (8) Septimiu Crisan, I.G. Târnovan, T.E.Crisan, "Vein pattern recognition. Image enhancement and feature extraction algorithms", 15th IMEKO TC4 Symposium, Iași, Romania, 2007, ISBN 978-973-667-260-6
- (9) Shi Zhao, Yiding Wang and Yunhong Wang, "Extracting Hand Vein Patterns

- from Low-Quality Images: A New Biometric technique Using Low-Cost Devices”, IEEE, 4th International Conference on Image and Graphics, 2007
- (10) Shi Zhao, Yi-Ding Wang and Yun-Hong Wang, "Biometric identification Based on Low Quality Hand Vein Pattern images", International Conf. on Machine Learning & Cybernetics, 12-15 July 2008, Kunming, Yunnan, China, Vol. 2, pp. 1172-1177.
  - (11) J.T. Kuenstner and K.H. Norris, “Spectrophotometry of human hemoglobin in the near infrared region from 1000 to 2500 nm”, J Near Infrared Spectroscopy 2 (1994), pp. 59–65.
  - (12) D. J. Faber, M. C. G. Aalders, E. G. Mik, B. A. Hooper, M. J. C. van Gemert, and T. G. van Leeuwen, “Oxygen Saturation-Dependent Absorption and Scattering of Blood.” Phys. Rev. Lett. 93, 028102 (2004).
  - (13) S. Srinivasan, B. W. Pogue, S. Jiang, H. Dehghani, and K. D. Paulsen, “Validation of hemoglobin and water molar absorption spectra in near-infrared diffuse optical tomography,” in Optical Tomography and Spectroscopy of Tissue V, B. Chance, R. R. Alfano, B. J. Tromberg, M. Tamura, and E. M. Sevick-Muraca, eds., Proc. SPIE 4955, 407– 415 (2003).
  - (14) S. L. Jacques, D. J. McAuliffe, "The melanosome: threshold temperature for explosive vaporization and internal absorption coefficient during pulsed laser irradiation," Photochemistry & Photobiology, 53, 769-75 (1991).
  - (15) Tabulated data from various sources compiled by S. Prahl at <http://omlc.ogi.edu/spectra>.

## List of Patent References

<b>No.</b>	<b>Patent No.</b>	<b>Country</b>	<b>Title</b>	<b>Inventors/Applicants</b>
1.	US D566,283	USA	Vein imaging apparatus	Brafford et al.
2.	220894	India	Imaging System using Diffuse Infrared Light	Luminetx Corporation
3.	US 7,239,909 B2	USA	Imaging System using Diffuse Infrared Light	Herbert D. Zeman
4.	WO 2004/080276 A2	International	Imaging System using Diffuse Infrared Light	Herbert D. Zeman
5.	1020050115275	Korea	Imaging System using Diffuse Infrared Light	Herbert D. Zeman
6.	AU 2004220644 B2	Australia	Imaging System using Diffuse Infrared Light	Herbert D. Zeman
7.	5357/CHENP/2009	India	System and Method for Projection of subsurface structure onto an object's surface	Luminetx Corporation
8.	WO 2008/101129 A1	International	System and Method for Projection of subsurface structure onto an object's surface	Luminetx Corporation
9.	5146923	USA	Apparatus and method for skin lesion examination	Atam P. Dhawan

## **Annexure I : Radiant power Energy Meter Details**

The annexure is received from the user guide of the Radiant power Energy Meter, from Spectra - Physics, Oriel Electronics.(Model 70260)

### **II.3 Photodiode Heads**

#### **Use of 70260 with Photodiode heads**

To set type of light source or Laser being used :

1. From bargraph measurements screen press the menu button twice and press “laser” until the correct laser type of wavelength is displayed.
2. Return to bargraph screen by pressing the menu button again.

#### **To choose manual or automatic ranging or dBm in power measurement :**

1. From the bargraph screen, press the menu button once.
2. Press “range” and then select the appropriate manual range autorange or dBm(logarithmic scale).
3. Press “exit” and then press the menu button twice to return to the bargraph measurement screen.

#### **Selecting chosen Wavelengths**

1. From the power measurement mode, press the menu button located on the right side until “more” appears. Press “more”.
2. Press select until “wavelength” is highlighted. Press “go”
3. Press “change” and then “up” and “down” to select the first wavelength. Repeat steps 2 and 3 for other wavelengths desired.

#### **Setting Startup Configurations**

1. From the power measurement mode press the menu button located on the right side until “more” appears. Press “more”.
2. Press “select” until “configure” is highlighted. Press “go”.
3. Press “select” until configure is highlighted. Press “go”.
4. Press “select” and “value” to choose the manual power range you wish to be default or choose autorange.
5. Now press “select’ and “value” again to choose the power line frequency and startup wavelength.

#### ***Power Measurement***

***Warning:*** Do not exceed the maximum head limit for power, energy, and power density as listed in the table with the head specifications. Otherwise, there is a risk of damaging the absorber.

**To expand the bargraph scale 10% about the present reading:**

1. From the bargraph power measurement screen press the menu button then press “zoom” then press the menu button twice again or simply press the center button from the bargraph screen without the menu button.
2. Press “zoom” again to return to full scale.

**To offset current reading set to zero:**

1. From the bargraph power measurement screen press the menu button then press “offset” or just press the left upper button from the bargraph screen.
2. Press “offset” again to cancel.

**To use the 70260 to fine tune light source or laser power:**

1. From the bargraph power measurement screen press the menu button twice then press “more”.
2. Press “select” until “tune” is highlighted. Press “go”.

**V. OPERATION WITH PHOTODIODE TYPE HEADS**

***Warning :***

*Before using the head for power or energy measurement, check that your light source or laser power or energy density does not exceed the head ratings*

**VI.1 Photodiode Absorber Heads**

When a photon source, such as a laser, is directed at a photodiode detector, a current is created proportional to the light intensity and dependent on the wavelength.

The 70286 heads and 70288 have a unique sensor design head (patent applied for) in which the two sensors are identical and connected back to back. When a uniform signal, such as room light, falls on the detector head the signal from the two sensors cancels.

On the other hand when a light source or a laser beam falls on the head, it illuminates only the first sensor and therefore is detected. Thus the 70286 automatically subtracts most of the background while detecting the desired signal. The subtraction is not perfect but usually 98% of the background signal is eliminated so that the detector can be easily be used in ordinary lighting conditions.

70282 Si head without background subtraction extends measurement capabilities to UV and 70287 be lead to IR.

The 70260 unit amplifies this signal and indicates the power level received by the head. Due to superior circuitry of the 70260, the noise level is very low, and the 70286 with the 70260 display has a large dynamic range from nano watts to hundreds of milliwatts.

Since many low power lasers have powers on the order of 5 to 30 mW, and most photo diode detectors saturate at about 2mW, the 70286 has been constructed with a built in filter so the basic head can measure to 30 mW without saturation. When the additional filter is installed, the maximum power is on the order of 300mW. The 70286 saturate when the output current exceeds 1mAso the exact minimum power depends on the sensitivity of the detector at the wavelength used. Section IV.2 Table gives the actual maximum power as a function of wavelength.

## **Annexure II: Diode Details**

3 Sets of LEDs used independently.

Wavelengths:

<b>No.</b>	<b>Wavelength</b>	<b>LED</b>	<b>Voltage(V)</b>	<b>Current(mA)</b>
1.	780nm	LED780-03AU	1.75	50
2.	840nm	ELD-840-515	1.7	10
3.	940nm	OPE5584S	14	100
4.	940nm	IR333C-A	1.1	20

The laser diodes were procured from

### **ROITHNER LASERTECHNIK GmbH**

Wiedner Hauptstrasse 76, A-1040 Vienna, Austria

Tel.: +43-1-5865243-0 Fax: +43-1-586524344

www.roithner-laser.com, office@roithner-laser.com

UID: ATU61938489, FN: 266954f, HG Wien

Customer no.: 133213

RLT Order no.: 027154